

Dual-Band Quad-Element Minimized MIMO 5G Smartphone Antenna for Sub-6 GHz Applications

Chuanba Zhang, Shuqi Xi, Lingrong Shen, Tian Hong Loh, *Senior Member, IEEE*, and Gui Liu, *Member, IEEE*

Abstract—A quad-element multiple-input multiple-output (MIMO) antenna operating in 3.5 GHz (3.4 GHz - 3.6 GHz) and 4.9 GHz (4.8 GHz - 4.96 GHz) frequency bands for the fifth-generation (5G) smartphone applications is presented. Each single radiating element consists of an L-shaped strip and a modified C-shaped strip. To keep enough space for second-, third- and fourth-generation (2G/3G/4G) antennas in a limited space, four antenna elements are printed respectively at four corners of a system board. The total size of the proposed antenna is only $145 \times 75 \times 5 \text{ mm}^3$. The design steps and the analysis of key parameters of an individual antenna element are derived to demonstrate the design methodology of the proposed antenna. The measured total radiation efficiency is better than 60% at both the operating frequency bands. The measured isolation is better than 16 dB and the calculated envelope correlation coefficient (ECC) is smaller than 0.02. The measured results demonstrate that the proposed MIMO antenna is a good alternative for sub-6 GHz 5G smartphone applications.

Index Terms—MIMO antenna, 5G, Dual bands, minimized dimension.

I. INTRODUCTION

After the 3.5 GHz (3.3 GHz - 3.8 GHz) frequency band was allocated as one of the fifth-generation (5G) mobile phone spectrums, a booming development of 5G multiple-input-multiple-output (MIMO) antenna has been experienced over the past few years. The 4.9 GHz (4.8 GHz - 4.96 GHz) frequency band was also taken into the consideration of 5G massive MIMO antenna designs. The Chinese government has approved two frequency bands between 3.3 GHz to 3.6 GHz and 4.8 GHz to 4.96 GHz as the sub-6 GHz frequency bands, which have greatly promoted the development of 5G MIMO antennas. Recently, many 5G MIMO antennas for sub-6 GHz smart phone applications have been proposed [1-16]. However, due to the limited internal space of mobile terminals, it is very challenging to integrate as many antenna elements within the mobile handset with excellent isolation and lower envelope correlation coefficient (ECC). There are a

few methods to decrease the unwanted coupling between antenna elements in a MIMO system, such as defected ground structure [3], isolation structure [4], neutral line [5], high-pass filter [9] and metamaterial structure [10]. In [7], a dual-band 4×4 MIMO antenna array was explored whereby isolation larger than 15 dB between the four elements was achieved by large separation distance between the elements. However, the dimension of a single element is relative large ($15 \text{ mm} \times 7 \text{ mm}$). A dual-band eight-element MIMO antenna with neutral line for 5G smartphone was presented in [5]. Two antenna elements were fabricated at the metallic side frames. A short neutral line was employed to decrease the coupling and excellent isolation of larger than 28 dB and 17 dB were realized at 3.5 GHz and 4.6 GHz, respectively.

Since almost all side boards of the above 5G smartphone antenna designs are higher than 6 mm, which does not support towards the implementation of ultra-thin antennas in the upcoming 5G mobile handset product. In [15], a low-profile high isolation 8-element 5G mobile antenna was demonstrated. Without any auxiliary decoupling technology, the worst isolation between elements was even better than 20 dB. Compared with the other reported 5G MIMO antennas, its apparent merit is the low-profile of 5.3 mm thickness.

In this paper, a low-profile quad-element dual-band 5G MIMO antenna operating at 3.5 GHz and 4.9 GHz bands is presented. The total dimension of the antenna is only $145 \times 75 \times 5 \text{ mm}^3$. For the sake of validating the simulated results, a prototype of the presented MIMO antenna was fabricated. The measured results, such as the S-parameters, total radiation efficiency, two-dimensional (2D) radiating pattern, and the calculated ECCs are manifested. Furthermore, the impact due to user's hand has also been investigated to assess the robustness of the proposed antenna. The primary highlights of the presented antenna are its low profile and high isolation, which is suitable for applications in emerging ultra-thin smartphone terminals.

II. ANTENNA DESIGN

The overall geometry and detailed design of the presented dual-band quad-element antenna for 5G smartphone applications is demonstrated in Fig. 1. The printed circuit boards (PCBs) of the presented system include a main system circuit board ($145 \times 75 \times 0.8 \text{ mm}^3$) and two side boards ($145 \times 4.2 \times 0.8 \text{ mm}^3$),

The work was funded in part by National Natural Science Foundation of China under Grant No. 61671330, Science and Technology Department of Zhejiang Province under Grant No. LGG19F010009, and Wenzhou Municipal Science and Technology Program under Grant No. 2018ZG019 and No. C20170005. The work of T. H. Loh was supported by the 2021 - 2025 National Measurement System Programme of the UK government's Department for Business, Energy and Industrial Strategy (BEIS), under Science Theme Reference EMT22 of that Programme. (Corresponding author: Gui Liu, e-mail: gliu@wzu.edu.cn).

C. Zhang, S. Xi, L. Shen and G. Liu are with College of Electrical and Electronic Engineering, Wenzhou University, Wenzhou 325035, China.

T. H. Loh is with Electromagnetic & Electrochemical Technologies Department, National Physical Laboratory, Teddington, Middlesex TW11 0LW, United Kingdom.

> REPLACE THIS LINE WITH YOUR MANUSCRIPT ID NUMBER (DOUBLE-CLICK HERE TO EDIT) <

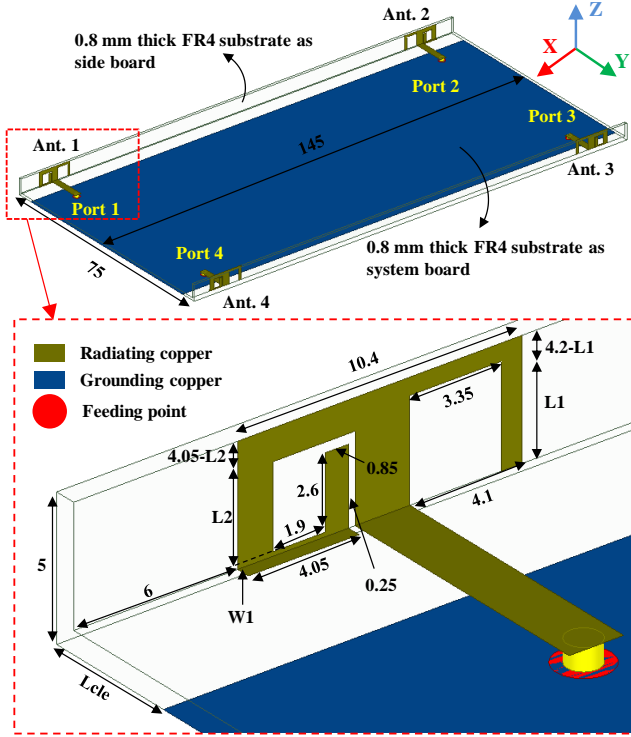


Fig. 1. Overall geometry and dimensions of the presented dual-band quad-element antenna array (dimension in millimeters).

which is smaller than a typical size for a 5.5 inch smart phone ($150 \times 75 \times 7 \text{ mm}^3$). All the PCBs are fabricated on a FR4 substrate with thickness of 0.8 mm, dielectric constant ϵ_r of 4.4 and loss tangent $\tan \delta$ of 0.02. The system ground plane ($145 \text{ mm} \times 65 \text{ mm}$) is printed on the back side of the main system circuit board. The quad antenna elements are printed on the inner side of the two side boards, which are placed vertically to the main system circuit board. As shown in Fig. 1, each antenna element is fed by a $50\text{-}\Omega$ microstrip feedline and a SMA connector through via-hole from the back of the main system circuit board. The size of the feedline is $10 \text{ mm} \times 2 \text{ mm}$. The detailed structure of a single antenna element is indicated in Fig. 1. Each single antenna element consists of an L-shaped strip and a modified C-shaped strip.

III. ANTENNA ANALYSIS

In order to gain the insight understanding on the presented antenna array, the design methodology, distributions of surface current and electric field at two resonant frequencies, three critical parameters analysis and a single-hand mode (SHM) are studied and presented in this section.

A. Design Evolution of the Proposed Antenna

The evolutionary steps of the presented antenna array element and the corresponding simulated reflection coefficients are shown in Fig. 2(b). As shown in Fig. 2(a), Step 1 is a simple T-shaped monopole structure that can cover only the upper band between 4.8 GHz and 5 GHz. In Step 2,

by adding two rectangle strips to antenna element in Step 1, it is clear that the resonant frequency was shifted toward lower

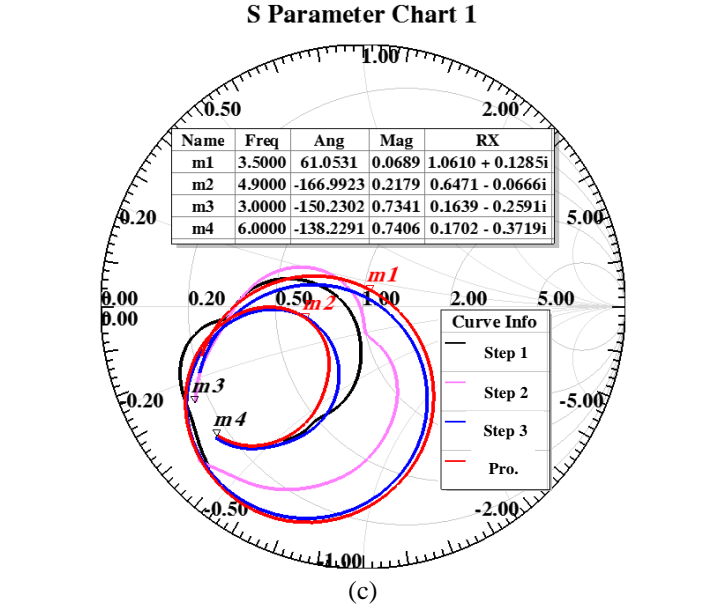
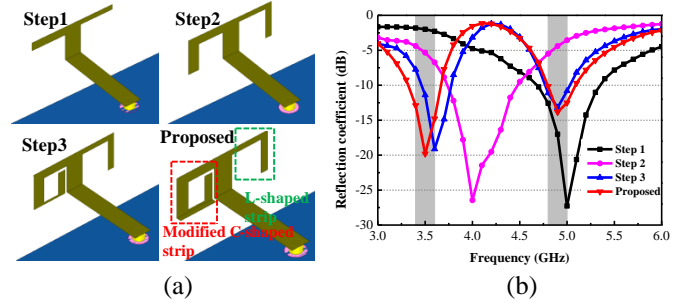


Fig. 2. Evolution process of a single antenna element. (a) the design steps of an antenna element; (b) the reflection coefficients of the relevant antenna element at each design step; (c) simulated Smith Chart of the device at various procedure.

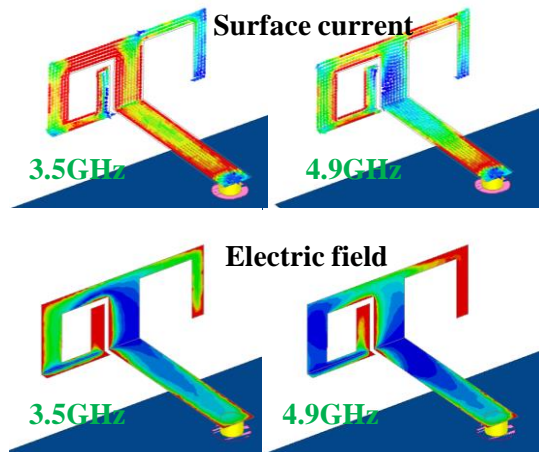


Fig. 3. Simulated surface current and electric field distribution.

frequencies. The simulated input return loss for both Step 1 and Step 2 show that the relevant antenna element operates with a single frequency band. In Step 3, an L-shaped strip was added to the left lower section of antenna element in Step 2,

> REPLACE THIS LINE WITH YOUR MANUSCRIPT ID NUMBER (DOUBLE-CLICK HERE TO EDIT) <

whereby the result shows that the relevant antenna can operate with two frequency bands. The -10 dB impedance frequency bands are between 3.48 GHz to 3.75 GHz and between 4.76 GHz to 5.08 GHz. It is obvious that the lower frequency band does not meet the requirement.

A novel antenna element is presented by adding a rectangle strip in the bottom strip of Step 3. The proposed antenna element can cover two desired frequency bands. The final structure of the proposed antenna element is composed of a modified C-shaped strip and an L-shaped strip. The modified C-shaped made a contribution to the lower working band, while the higher operating frequency band is mainly affected by the L-shaped strip, which will be discussed in later section. Fig. 2(c) provides the simulated impedance Smith chart of each design procedure. It is noteworthy that the normalized impedance smith curves of different step are gradually approaching to the center of the smith chart circle. Marker m1 and m2 are two resonant frequencies of the final structure. The simulated normalized port impedance at two resonant modes is $1.06+0.13$ and $0.65-0.07i$, respectively, preferable and acceptable impedance matching conditions are obtained at both 3.5 GHz and 4.9 GHz.

B. Analysis of the Surface Current and Electric Field Distribution of the Proposed Antenna Element

To verify the difference of the proposed structure of antenna elements, the current distribution and electric field at the two resonant frequencies (3.5 GHz and 4.9 GHz) are plotted, respectively. As depicted in Fig. 3, the surface current at 3.5 GHz is mainly concentrated at the modified C-shaped strip. At 4.9 GHz, the strongest current intensity is observed at the upper proportion of the L-shaped strip and the inner round of the modified C-shaped strip. On the contrary, the simulated electric field is mainly distributed at the position of low current density.

C. Analysis of the Variables of the Proposed Antenna

To validate that the modified C-shaped strip is responsible for the excitation of the lower resonant mode and the introduction of L-shaped strip is for the higher operation band, further parametric analyses are introduced. When one parametric is analyzed, all the other parameters keep constant. As shown in Fig. 4(a), the lower working frequency band is shifted to lower frequencies with the increase of $W1$, but $W1$ has a little influence upon the higher working frequency band. The optimized value of $W1$ is 0.5 mm, and the -10 dB impedance band of the lower operating frequency is 3.3 GHz - 3.68 GHz, which can cover the desired frequency band between 3.4 GHz - 3.6 GHz. The impact of an L-shaped strip on antenna performance is demonstrated in Fig. 4(b). It is obvious that the upper frequency band is moved to higher frequencies and the lower frequency band is almost not affected at all when $L1$ increases. The most suitable value of $L1$ is 3.6 mm, and the corresponding -10 dB impedance frequency band of the upper band is 4.77 GHz - 5.08 GHz. The length of $L2$ has an obvious effect on both operating frequency bands, which is depicted in Fig. 4(c). When the

value of $L2$ decreases, both two frequency bands are shifted towards higher frequencies. The optimum value of $L2$ is 2.95 mm. Fig. 4(d) manifests the effect of the dimension of ground clearance on antenna performance. When the width of ground clearance (L_{cle}) decreases, two resonant frequencies are slightly shifted toward lower or higher frequencies, while the input impedance matching at 3.5 GHz deteriorates significantly. After proper optimization, this design precisely resonating at 3.5 GHz and 4.9 GHz when L_{cle} equals to 5.0 mm.

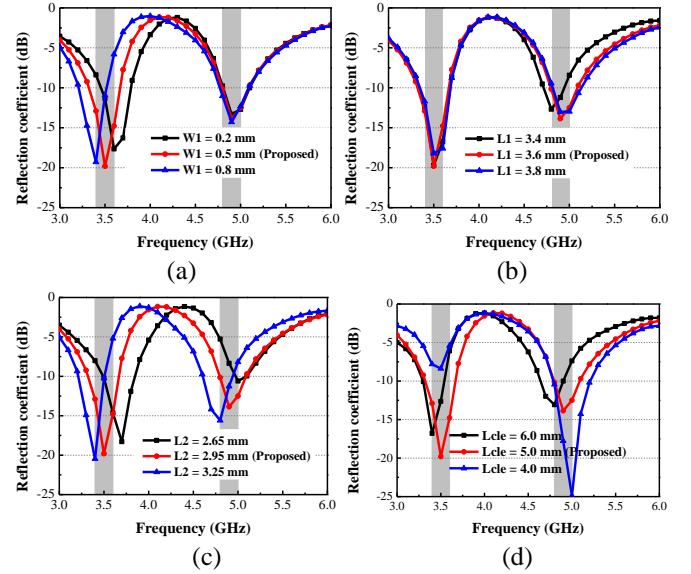


Fig. 4. Simulated reflection coefficient with various (a) $W1$; (b) $L1$; (c) $L2$; (d) L_{cle} .

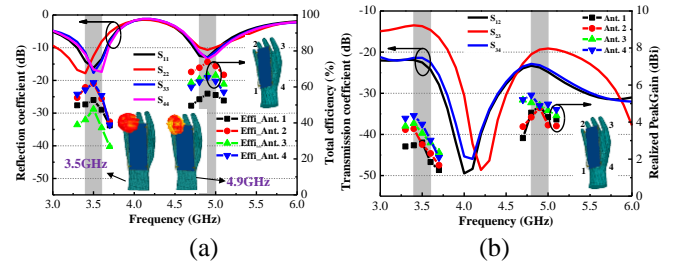


Fig. 5. Simulated results when this device is held in SHM. (a) reflection coefficient and total efficiency; (b) transmission coefficient and realized peak gain.

D. Analysis of A Simulated Application Scenario of the Propose Antenna

Fig. 7 depicts an application scenario of single hand mode (SHM). The simulated S-parameters are also exhibited. When the smartphone is held in SHM, the -10 dB impedance bandwidths of Ant. 2 (see Fig. 5(a)) deteriorate due to the most adjacent of the hand model. However, the simulated -10 dB impedance bandwidths of others can still cover both operating bands. The isolation values are larger than 13 dB, as illustrated in Fig. 5(b), the worst isolation appeared between Ant. 2 and Ant. 4. When this device is held in SHM, the simulated maximum total efficiency and peak gain in the higher band are 72% and 5.5 dBi, respectively. The simulated three-dimensional (3D) radiating patterns of one antenna

> REPLACE THIS LINE WITH YOUR MANUSCRIPT ID NUMBER (DOUBLE-CLICK HERE TO EDIT) <

element at two resonant frequencies are also pasted in Fig. 5(a).

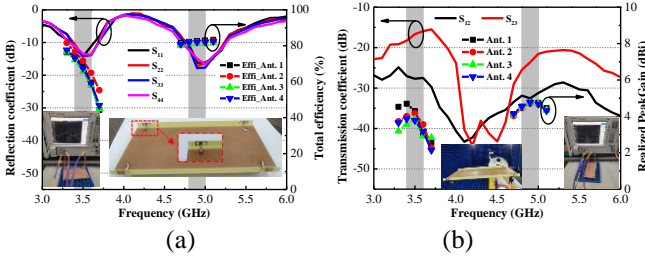


Fig. 6. Measured S-parameters results of the proposed antenna: (a) reflection coefficients and total efficiency; (b) transmission coefficients and realized peak gain.

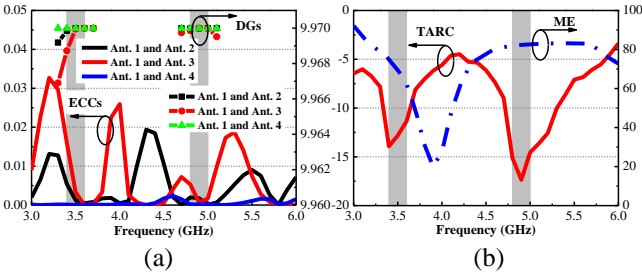


Fig. 7. Computed ECCs, DGs, TARC and ME: (a) ECCs and DGs; (b) TARC and ME.

IV. EXPERIMENTAL RESULTS AND DISCUSSION

To validate the simulated results of the presented MIMO antenna, a prototype was manufactured and tested. Fig. 6 shows the measured S-parameters, total efficiency and realized peak gain. The S-parameters are measured by Keysight Vector Network Analyzer N5224A. The measured -10 dB impedance bandwidth are 3.38 GHz - 3.64 GHz and 4.78 GHz - 5.22 GHz, which can fully cover both desired bands. The measured isolation are greater than 16 dB and 22 dB at the lower and upper frequency band, respectively. The slight frequency offset is envisaged due to the manufacturing tolerance. The measured total radiation efficiencies of each element are better than 60%. The measured realized peak gain of each element at 3.5 GHz and 4.9 GHz is 4.6 dBi and 5 dBi, respectively. Fig. 8 presents the measured 2D radiating pattern of the proposed antenna at 3.5 GHz and 4.9 GHz. The measured co-polar and cross-polar plots are represented by black solid and red solid lines, respectively. The left column represents 2D radiation pattern in x-o-y plane, and the right column represents 2D radiation pattern in x-o-z plane.

In order to further prove the MIMO performance of the proposed antenna. The ECCs, diversity gain (DG) are calculated and provided in Fig. 7(a). Obviously, the computed ECC values are well below 0.02 in both desired bands, and the DGs are larger than 9.966 in the operating bands, which can well support the 5G handset. The total active reflection coefficient (TARC) is also a crucial index for elevating the MIMO antenna diversity performance. TARC is defined the ratio of square root of total reflected power divided by the total incident power [16]. The calculated TARC and the multiplexing efficiency (ME) are depicted in Fig. 7(b). The

calculated TARC at the two operating bands are lower than 11 dB and 14 dB, respectively. The corresponding ME are larger than 60% and 80% at 3.4 GHz - 3.6 GHz and 4.8 GHz - 4.96 GHz, which proved excellent diversity performance.

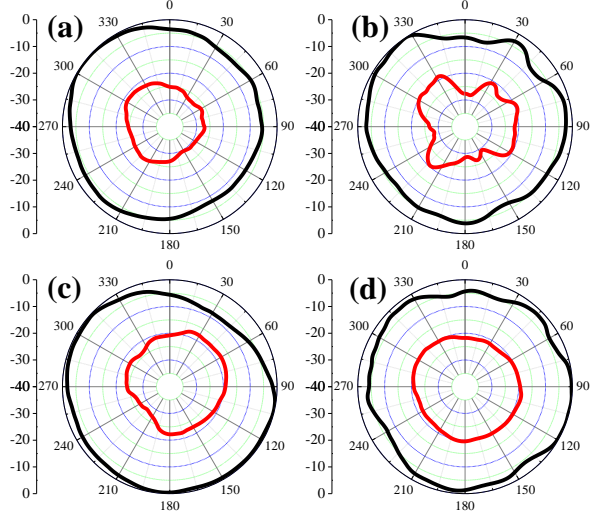


Fig. 8. Measured 2D radiation patterns of the proposed quad-element MIMO antenna: (a) 3.5 GHz x-o-y plane; (b) 3.5 GHz x-o-z plane; (c) 4.9 GHz x-o-y plane; (d) 4.9 GHz x-o-z plane.

TABLE I
COMPARISONS OF 5G SMARTPHONE ANTENNAS

Design	Bandwidth (GHz)	Isolation (dB)	Eff. (%)	ECC	Unit size (mm ³)
[5]	3.4-3.6(-10dB)	28	45-75	0.05	16.5×6
	4.5-4.75(-10dB)	17	52-80		
[6]	3.4-3.6(-10dB)	16.5	85	0.01	15×7×0.8
	4.6-4.9(-10dB)	20	82		
[7]	3.3-3.8(-10dB)	15	70	0.02	14.9×7×0.8
	4.6-4.75(-10dB)				
[8]	3.4-3.6(-6dB)	11.5	41-72	0.08	15×7×0.8
	4.8-5.1(-6dB)	14	40-85		
This work	3.4-3.6(-10dB)	16	60-77	0.02	10.4×4.2×0.5
	4.8-5.0(-10dB)	22	80		

Table I shows a performance comparison between the proposed antenna and other 5G published papers recently. By contrast with other designs, the proposed antenna element has the comparative minimum volume, excellent isolation performance. The highlight of our work is that we have proposed a low-profile, excellent isolation, lower ECCs MIMO antenna suitable for application to emerging ultra-thin 5G handset smartphones.

V. CONCLUSION

In this paper, a dual-band 4-element antenna array operating at 3.5 GHz and 4.9 GHz frequency bands for 5G mobile handset applications is proposed. The dimension of the MIMO antenna is only 145 × 75 × 5 mm³. Without any auxiliary decoupling branches, the measured worst isolation was larger than 16 dB. Besides, lower ECCs and high total efficiency are obtained. Great MIMO diversity performance is also realized. The application scenario of SHM is also provided. The proposed design is a candidate suitable to be utilized in the applications of sub-6 GHz 5G smartphones.

REFERENCES

- [1] Y. Li, C. Sim, Y. Luo and G. Yang, "High-Isolation 3.5 GHz Eight-Antenna MIMO Array Using Balanced Open-Slot Antenna Element for 5G Smartphones," *IEEE Trans. Antennas Propag.*, vol. 67, no. 6, pp. 3820-3830, June. 2019.
- [2] X. Zhang, Y. Li, W. Wang and W. Shen, "Ultra-Wideband 8-Port MIMO Antenna Array for 5G Metal-Frame Smartphones" *IEEE Access*, vol. 7, pp. 72273-72282, 2019.
- [3] J. Li, X. Zhang, Z. Wang, "Dual-Band Eight-Antenna Array Design for MIMO Applications in 5G Mobile Terminals," *IEEE Access*, vol. 7, pp. 71636-71680, 2019.
- [4] L. Cui, J. Guo, Y. Liu and C. -Y. -D. Sim, "An 8-Element Dual-Band MIMO Antenna with Decoupling Stub for 5G Smartphone Applications," *IEEE Antennas Wireless Propag. Lett.*, vol. 18, no. 10, pp. 2095-2099, Oct. 2019.
- [5] X. Shi, M. Zhang, S. Xu, D. Liu, H. Wen and J. Wang, "Dual-Band 8-Element MIMO Antenna with Short Neutral Line for 5G Mobile Handset," in *EUCAP*, Pairs, France, 2017, pp. 3140-3142.
- [6] J. Huang, G. Dong, J. Cai, H. Li and G. Liu, "A Quad-Port Dual-Band MIMO Antenna Array for 5G Smartphone Applications," *Electronics*, no. 5, pp. 542-547, Feb. 2021.
- [7] J. Huang, G. Dong, Q. Cai, Z. Chen, L. Li and G. Liu, "Dual-Band MIMO Antenna for 5G/WLAN Mobile Terminals," *Micromachines*, no. 12, pp. 489-501, Apr. 2021.
- [8] J. Guo, L. Cui, C. Li and B. Sun, "Side-Edge Frame Printed Eight-Port Dual-Band Antenna Array for 5G Smartphone Applications" *IEEE Trans. Antennas Propag.*, vol. 66, no. 12, pp. 7412-7417, Dec. 2018.
- [9] F. Xiao, X. Lin and Y. Su, "Dual-Band Structure-Shared Antenna with Large Frequency Ratio for 5G Communication Applications" *IEEE Antennas Wireless Propag. Lett.*, vol. 19, no. 12, pp. 2339-2343, Dec. 2020.
- [10] Z. Xu and C. Deng, "High-Isolated MIMO Antenna Design Based on Pattern Diversity for 5G Mobile Terminals" *IEEE Antennas Wireless Propag. Lett.*, vol. 19, no. 3, pp. 467-471, March. 2020.
- [11] L. Sun, Y. Li, Z. Zhang and H. Wang, "Self-Decoupled MIMO Antenna Pair with Shared Radiator for 5G Smartphones" *IEEE Trans. Antennas Propag.*, vol. 68, no. 5, pp. 3423-3432, May. 2020.
- [12] A. Iqbal, O. A. Saraereh, A. Bouazizi, A. Basir, "Metamaterial-Based Highly Isolated MIMO Antenna for Portable Wireless Applications" *Electronics*, no. 7, pp. 267, Oct. 2018.
- [13] L. Sun, Y. Li, Z. Zhang and Z. Feng, "Wideband 5G MIMO Antenna with Integrated Orthogonal-Mode Dual-Antenna Pairs for Metal-Rimmed Smartphones," *IEEE Trans. Antennas Propag.*, vol. 68, no. 4, pp. 2494-2503, April. 2020.
- [14] A. Zhao and Z. Ren, "Size Reduction of Self-Isolated MIMO Antenna System for 5G Mobile Phone Applications" *IEEE Antennas Wireless Propag. Lett.*, vol. 18, no. 1, pp. 152-156, Jan. 2019.
- [15] R. Li, Z. Mo, H. Sun, X. Sun, Du, G, "A Low-Profile and High-isolated MIMO Antenna for 5G Mobile Terminal," *Micromachines*, no. 11, pp. 360-371, Mar. 2020.
- [16] M. Sharawi, M. Khan, A. Numan and D. Aloï, "A CSRR Loaded MIMO Antenna System for ISM Band Operation," *IEEE Trans. Antennas Propag.*, vol. 61, no. 8, pp. 4265-4274, Aug. 2013.